

Mesososcopic modeling of flow and dispersion phenomena in fractured solids

V.K. Michalis^{a,b}, A.N. Kalarakis^a, E.D. Skouras^a, V.N. Burganos^{a,*}

^a *Institute of Chemical Engineering and High Temperature Chemical Processes, Foundation for Research and Technology, Hellas, Greece*

^b *Department of Chemical Engineering, University of Patras, Patras, Greece*

Abstract

The problem of hydrodynamic dispersion in porous media is considered and numerical predictions of the mixing degree in a single intersection are provided. The flow field in the intersection and adjacent pores or fractures is calculated using a lattice Boltzmann model for single phase flow. A particle-tracking scheme is used, subsequently, that monitors the migration of solute particles in the area of the intersection taking into account the local flow field and a Brownian field. Mixing is quantified in terms of the probability of solute transfer across the junction into the opposite fracture. To circumvent the problem of large computational times for cases of fast flow compared to diffusion, a lattice Boltzmann advection–diffusion model is used, that offers significant savings on computational time without sacrificing accuracy. It is shown that the solute dispersion in a fracture network is a strong function of the Reynolds number, even if the Peclet number remains constant, due to the extensive recirculation areas that may develop in regions close to the junction.

© 2007 Elsevier Ltd. All rights reserved.

Keywords: Lattice Boltzmann; Dispersion; Mixing; Particle tracking

1. Introduction

Hydrodynamic dispersion in microscopically inhomogeneous media, such as porous solids, is a phenomenon of particular importance in modern industrial and environmental applications, including miscible displacements in enhanced oil recovery, salt water intrusion in coastal aquifers, remediation schemes for contaminated groundwater, separation processes, and radioactive waste disposal. The migration of solvable tracers or contaminants in porous media under inert conditions and in the absence of phase transition is the result of the combined action of convective flow and molecular diffusion in the pore domain. A detailed understanding of the dispersion process is essential for predicting the transport and fate of species under a variety of conditions and parameters.

The usually complex structure of the solid renders the study of dispersion a difficult task and necessitates the introduction of several simplifying assumptions. A common approach is based on the assumption that the void space can be represented by a discrete network of passages, and is particularly popular in the case of fractured rocks or

* Corresponding author.

E-mail address: vbur@iceht.forth.gr (V.N. Burganos).

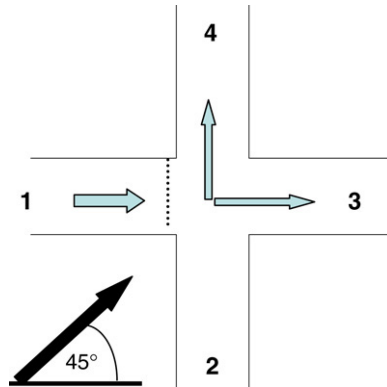


Fig. 1. Schematic representation of an orthogonal intersection, indicating the macroscopic flow direction. The carrier fluid enters through inlet branches 1 and 2, and exits through outlet branches 3 and 4. The dotted line shows a choice of the position of the solute pulse in dispersion calculations.

synthetic materials. Such a network representation has inspired a great amount of work with not only theoretical but also experimental emphasis, as in the case of pore networks etched in glass [16]. Even though the discrete network models use, typically, a large number of individual pores, it is widely accepted that flow and transport within a *single pore intersection* affect dispersion at the network scale. The need to understand the transport phenomena in a single intersection led to numerous publications of mixing at this scale. The two most common assumptions concerning mixing at the intersections are the complete mixing and the streamline-routing approximations. The first approach assumes complete homogenization of the incoming solute concentration within the intersection; thus, the concentration in the outlet branches is proportional to their volumetric fluxes. On the other hand, in the streamline-routing approach the diffusion mechanism is neglected and, consequently, the mass partitioning at the intersection is based only on the flow pattern. Between these two extreme cases lies the majority of practical applications, that are governed by combined convection and diffusion. The Peclet number shows the relative contribution of convective mass transport to diffusion and it can be defined as

$$Pe = v_0 l / D_m,$$

where v_0 is some mean fluid velocity, l is a characteristic length of the medium and D_m is the molecular diffusion coefficient. Streamline routing is valid only as $Pe \rightarrow \infty$ whereas complete mixing, which requires large residence time of solute at the intersection, is generally valid as $Pe \rightarrow 0$.

Several studies have been focused on the mixing at intersections, which is quantified by the “mixing ratio”. Fig. 1 shows the idealized case of an orthogonal intersection of two inlet and two outlet branches. In this case, the mixing ratio, M_r , is defined as the ratio of the solute flow rate in the outlet that is aligned with the inlet branch to the sum of the solute flow rates in the two outlet branches:

$$M_r = J_3 / (J_3 + J_4) \quad (1.2).$$

Berkowitz et al. [1] studied dispersion in orthogonal fractures with smooth walls, using the aforementioned mixing ratio. They solved the Stokes equation to evaluate the flow field and the particle-tracking method to calculate the M_r value in two dimensions. They concluded that mixing is incomplete for any value of the Peclet number.

Stockman et al. [36] used lattice gas and lattice Boltzmann methods to estimate the mixing ratios for Pe values ranging from 0 to 1547. For an orthogonal intersection of two identical fractures with equal flow rates, M_r approaches 0.5 for $Pe \approx 1$, indicating almost complete mixing. On the other hand, for high Pe values they obtained finite M_r values, suggesting that, even at such high Pe values, streamline routing cannot be the exclusive mechanism of solute transport.

Simple analytical solutions for the transfer probabilities of solute at an intersection were proposed by Park and Lee [31]. Their results are in satisfactory agreement with those by Stockman et al. [36], when corrected for longitudinal diffusion.

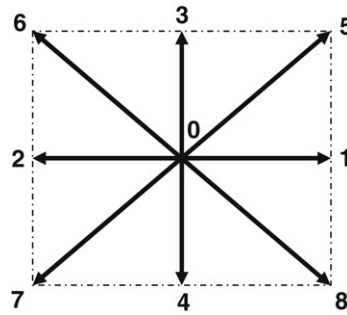


Fig. 2. Square cell involving nine velocity vectors, as used in lattice Boltzmann computations.

Li [25] proposed a linear combination of mechanical dispersion and molecular diffusion, and used a particle-tracking technique to evaluate M_r . He concluded that complete mixing may occur for $Pe < 1$ and that the mixing ratio practically vanishes for $Pe > 100$.

Mourzenko et al. [29] presented a numerical study of three-dimensional solute transport in fracture intersections and provided estimates of M_r for various Pe values, in slit-like channels with smooth or rough walls. They used the Stokes equation for the calculation of the flow field and a random walk method for the simulation of solute transport, similar to that by Berkowitz et al. [1]. It was concluded that the local Peclet number must be taken into account in large-scale simulations.

In the present work, the computation of the mixing ratio in orthogonal intersections of fractures that are inclined with respect to the macroscopic flow direction is achieved through a combination of a lattice Boltzmann (LB) method and a particle-tracking method. Results over a wide range of Pe values are obtained and used to evaluate the transverse dispersion coefficient. An alternative approach is also suggested, which uses an advection–diffusion lattice Boltzmann model and is also capable of providing estimates of the mixing ratio offering at the same time significant savings in computational time, especially for high Pe values where diffusion is of limited significance in the transport process. The incorporation of a forcing term in the LB model is discussed and an investigation of the effect of the boundary condition at the fluid–solid interface on solute transport is carried out.

2. Simulation method

Consider an orthogonal intersection of two identical fractures, as shown in Fig. 1. An incompressible Newtonian fluid enters the intersection through inlet branches 1, 2 and leaves through outlet branches 3, 4, carrying along a low concentration of solute particles. The fractures are assumed to be slit shaped, extending invariably to infinity in the third direction. Under conditions of laminar flow, which are usually valid in the interior of porous media, the two-dimensional Navier–Stokes and continuity equations suffice to describe the fluid motion at steady state. On the contrary, the stochastic motion of the solute particles necessitates the consideration of three-dimensional trajectories, though their projection onto the cross sectional x – y plane suffices to determine the quantities needed in this work.

2.1. Flow field calculation

The lattice Boltzmann (LB) method is employed to calculate the flow field. Two different lattices were used here, namely, the nine-speed [33] and the seven-speed [13] two-dimensional lattices, which resulted in quite similar, yet not identical, results. However, the nine-speed model proved advantageous over the seven-speed model as it facilitated the smoother construction of streamlines across the intersections. The nine unit-velocity vectors are depicted in Fig. 2, and are defined below [33]:

$$\mathbf{e}_0 = (0, 0) \quad (1)$$

$$\mathbf{e}_i = \left(\cos \frac{i-1}{2} \pi, \sin \frac{i-1}{2} \pi \right); \quad i = 1, \dots, 4 \quad (2)$$

$$\mathbf{e}_i = \sqrt{2} \left(\cos \frac{i-5}{2} \pi + \frac{\pi}{4}, \sin \frac{i-5}{2} \pi + \frac{\pi}{4} \right); \quad i = 5, \dots, 8. \quad (3)$$

The evolution of the system follows the LB equation

$$f_i(\mathbf{x} + \mathbf{e}_i, t + 1) = f_i(\mathbf{x}, t) + \Omega_i; \quad i = 0, \dots, 8, \tag{4}$$

where Ω_i is the collision operator. Introducing the single relaxation parameter τ (BGK approach by Bhatnagar et al. [4]) the collision operator can be approximated by the following expression [33]:

$$\Omega_i = -\frac{f_i - f_i^{\text{eq}}}{\tau}; \quad i = 0, \dots, 8. \tag{5}$$

The equilibrium distribution function is expanded around the local velocity [15,8,20]:

$$f_i^{\text{eq}} = w_i \rho \left(1 + \frac{1}{c_s^2} (\mathbf{e}_i \cdot \mathbf{v}) + \frac{1}{2c_s^4} (\mathbf{e}_i \cdot \mathbf{v})^2 - \frac{1}{2c_s^2} v^2 \right);$$

$$w_0 = \frac{4}{9}; \quad w_i = \frac{1}{9}, \quad i = 1, \dots, 4; \quad w_i = \frac{1}{36}, \quad i = 5, \dots, 8. \tag{6}$$

In the above equilibrium distribution function the speed of sound is

$$c_s = \frac{1}{\sqrt{3}}. \tag{7}$$

The local density and velocity of the LB particles are given by the following summations:

$$\rho(\mathbf{x}, t) = \sum_i f_i(\mathbf{x}, t) = \sum_i f_i^{\text{eq}}(\mathbf{x}, t) \tag{8}$$

$$\rho \mathbf{v}(\mathbf{x}, t) = \sum_i f_i(\mathbf{x}, t) \mathbf{e}_i = \sum_i f_i^{\text{eq}}(\mathbf{x}, t) \mathbf{e}_i. \tag{9}$$

The Navier–Stokes equation can be recovered from the LB equations using the Chapman–Enskog expansion [7,19]. The mass and momentum balance equations derived from Eqs. (4)–(9) are [33]:

$$\frac{\partial \rho}{\partial t} + \nabla \cdot (\rho \mathbf{v}) = 0 \tag{10}$$

$$\frac{\partial (\rho \mathbf{v})}{\partial t} + \nabla \cdot (\rho \mathbf{v} \mathbf{v}) = -\nabla P + \rho \mu \nabla^2 \mathbf{v} + O(v^3). \tag{11}$$

The corresponding kinematic viscosity for the D_2Q_9 model is:

$$\nu = \frac{2\tau - 1}{6}. \tag{12}$$

2.2. Boundary conditions and forcing term for the flow field simulations

No-slip conditions are imposed on the fracture walls and periodic conditions are implemented by driving the exiting particle populations back into the working domain through the opposite side. Flow is induced with the help of a force term, which is added in the LB equation [37,26] as follows,

$$f_i(\mathbf{x} + \mathbf{e}_i, t + 1) = f_i(\mathbf{x}, t) - \frac{f_i - f_i^{\text{eq}}}{\tau} - F_i; \quad i = 0, \dots, 8, \tag{13}$$

where

$$F_i = w_i \rho \frac{1}{c_s^2} (\mathbf{e}_i \cdot \mathbf{a}); \quad i = 0, \dots, 8. \tag{14}$$

Eq. (13) is the simplest way to introduce a body force (\mathbf{F}) in the LB approach. A more accurate approach has been presented by Ginzbourg and Adler [17], who added an additional term in the LB equation and proposed a redefinition of the fluid velocity due to an external body force (\mathbf{F}), as follows:

$$\rho \mathbf{v} = \sum_i f_i \mathbf{e}_i + m \mathbf{F}; \quad m = \frac{1}{2}. \tag{15}$$

In their work, they applied this correction only in the definition of the macroscopic fluid velocity, without affecting the equilibrium distribution probability, $f_i^{\text{eq}}(\rho, \mathbf{v}^*)$, that is,

$$f_i^{\text{eq}} = w_i \rho \left(1 + \frac{1}{c_s^2} (\mathbf{e}_i \cdot \mathbf{v}^*) + \frac{1}{2c_s^4} (\mathbf{e}_i \cdot \mathbf{v}^*)^2 - \frac{1}{2c_s^2} v^{*2} \right), \tag{16}$$

where \mathbf{v}^* is given by

$$\rho \mathbf{v}^* = \sum_i f_i \mathbf{e}_i. \tag{17}$$

Another approach, initially proposed by Buick and Greated [5], suggests that the momentum correction should also apply to the equilibrium distribution calculation, defining \mathbf{v}^* from

$$\rho \mathbf{v}^* = \sum_i f_i \mathbf{e}_i + m \mathbf{F}; \quad m = \frac{1}{2}. \tag{18}$$

In the present work, the method proposed by He et al. [18] and Luo [27] was used, which neglects the correction term ($F/2$) in the fluid momentum equation, that is,

$$\text{(method 1)} \quad \rho \mathbf{v} = \sum_i f_i \mathbf{e}_i.$$

The justification of this approach lies with the fact that the error that is introduced in the macroscopic continuity equation [17,14]

$$\frac{\partial \rho}{\partial t} + \nabla \cdot (\rho \mathbf{v}) = -\frac{\delta t}{2} \nabla \cdot \mathbf{F} \tag{19}$$

should be negligible for the spatially uniform body force employed here, as verified numerically by Ladd and Verberg [23].

In our simulations the body force magnitude was of the order of 10^{-5} or less and the corresponding fluid velocity magnitude at steady state was of the order of 10^{-3} . As a result, the correction term of Eq. (15) becomes practically negligible.

Nevertheless, in order to see how these corrections may affect the dispersion calculations, we investigated the performance of two alternative approaches, that incorporate the forcing term in different ways. Specifically, we used in both approaches the velocity correction of Eq. (18) and inserted this expression into the equilibrium density expression. The two approaches differ in the forcing term expression, which is given either by

$$\text{(method 2)} \quad F_i = w_i \frac{1}{c_s^2} (\mathbf{e}_i \cdot \mathbf{F}); \quad i = 0, \dots, 8$$

or by the one proposed in Guo et al. [14]

$$\text{(method 3)} \quad F_i = \left(1 - \frac{1}{2\tau} \right) w_i \left(\frac{1}{c_s^2} (\mathbf{e}_i - \mathbf{v}^*) + \frac{1}{c_s^4} (\mathbf{e}_i \cdot \mathbf{v}^*) \mathbf{e}_i \right) \cdot \mathbf{F}.$$

It should be stated that method 2 is also incorrect and is mentioned here only for the sake of investigation of its numerical accuracy compared to that of method 3. Table 1 shows the M_r predictions by the three approaches. It was found that the “correction” offered by method 3 to the simplified method 1 is less than about 0.2%.

The desired Reynolds number can be achieved either through the adjustment of the magnitude of the body force or through the adjustment of the kinematic viscosity value. The direction of the mean flow relative to the network orientation is defined through the adjustment of the direction of the acceleration vector, \mathbf{a} . In the present work, an angle of 45° between the mean flow direction and the principal axes of the network is assumed. A typical flow field in such an intersection is shown in Fig. 3.

Table 1
 M_r calculations using different forcing term approaches; $Re = 0.14$

Pe	M_r (method 1)	M_r (method 2)	Relative deviation from method 1	M_r (method 3)	Relative deviation from method 1
1	0.47467	0.47468	<0.01%	0.47466	<0.01%
1000	0.08809	0.08790	−0.216%	0.08821	0.136%

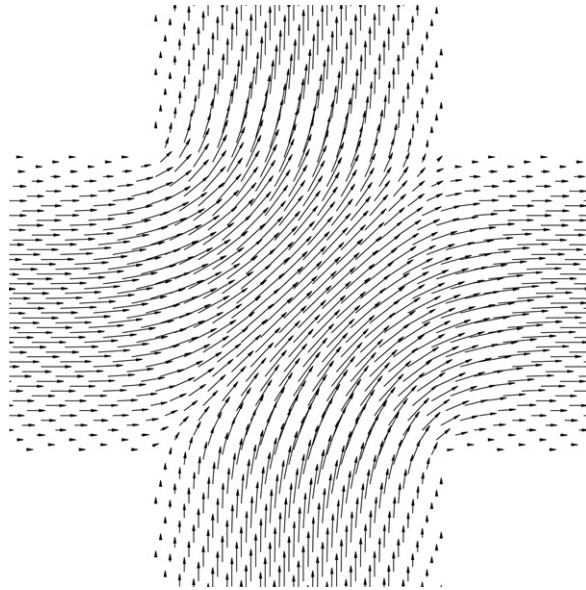


Fig. 3. Flow field in an orthogonal intersection. Lattice size: 205×205 . Fracture width-to-length ratio: 0.3.

The implementation of the no-slip solid–fluid boundary condition has been addressed in several LB publications. The simplest boundary condition assumes particle bounce back at the wall, which is located half way between the solid sites and the adjacent fluid sites. More complicated boundary conditions may improve accuracy in some cases. A Dirichlet-type boundary condition for the wall velocity (assigned to the fluid nodes adjacent to the wall, [21,39,30]) was also employed in this work and found to yield only slightly improved results compared to those obtained by the bounce-back method, and only for relatively small lattice sizes. For Poiseuille flow in a slit, the analytic solution of the velocity profile is known and therefore the error estimate is straightforward. In the case of the orthogonal junction the error estimate can be made by comparing the velocity profiles obtained with the bounce-back scheme and the second order scheme, and subsequently comparing the M_r values obtained using these flow fields. For the simulations considered in this paper the deviation was very small, namely less than 1%. For larger lattices, these small deviations are practically eliminated. Thus, it was decided to adopt the bounce-back approach throughout our computations to save on computational time. Nevertheless, care must be taken to ensure that the choice of the boundary condition in combination with the lattice size has a minimal effect on the solute particle trajectories, described below.

2.3. Particle tracking

The solute transport is simulated by the random walk approach. The individual trajectories of a large number of Brownian particles are calculated as the particles move within the intersection driven by both convection and diffusion. This kind of motion is implemented by the vectorial summation of the flow field and the stochastic Brownian diffusion field. At every elementary time step, the new position of the particle results from the summation of a displacement due to convection and a randomly oriented one due to diffusion

$$\delta \mathbf{r} = \mathbf{v}(\mathbf{r})\delta t + \delta \boldsymbol{\xi}. \quad (20)$$

The magnitude and direction of the local velocity vector, $\mathbf{v}(\mathbf{r})$, are obtained from the fluid flow field, offered by the LB method, appropriately transformed from lattice positions to off-lattice positions, \mathbf{r} , using a pixel-scale approximation.

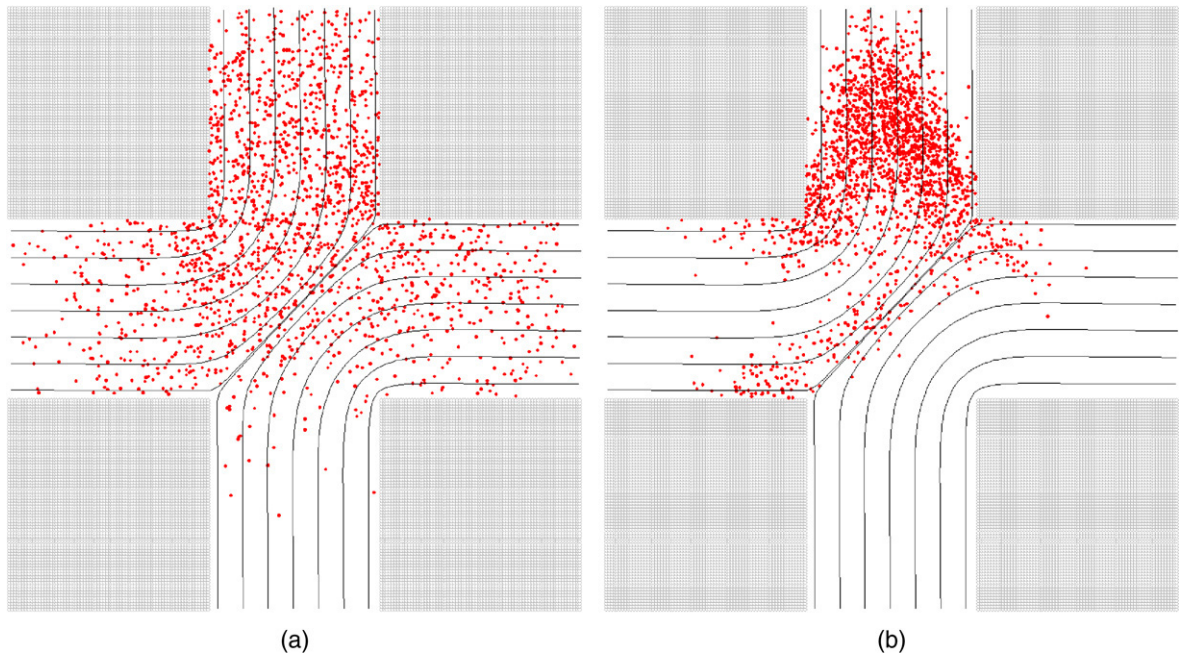


Fig. 4. Snapshots taken during the evolution of a solute pulse in an intersection, for two different Peclet number values. (a) $Pe = 10$, (b) $Pe = 100$. Dimensionless time = 0.42.

Specifically, the LB velocity is assumed to extend within a pixel around the node with side equal to the mesh size and a straightforward coordinate mapping is sufficient for the velocity read-out. The error introduced in this way is monitored and eventually limited to within a tolerance level through repeated calculations at progressively decreasing lattice constant. The magnitude of the random displacement vector $\delta\xi$ is related to the molecular diffusion coefficient through the equation

$$D_M = \frac{\delta\xi^2}{6\delta t}, \quad (21)$$

and, practically, represents the average displacement of Brownian walkers within the time interval δt .

This method (or some variant of it) has been used in several publications on dispersion in porous media (e.g., [28,29,3]). Numerical convergence requires that the elementary time step be neither too large to lose essential information of the spatial variation of the flow field, nor too small to render the method computationally unattractive. According to Salles et al. [34] a suitable compromise is

$$\delta r < \frac{b}{2}, \quad (22)$$

where b is the pixel size. In the present case, the pixel size is equal to the lattice unit, as this is defined in the LB flow field calculations. Upon collision with the fracture walls the particles are assumed to undergo a diffuse reflection [6].

In the definition of the Peclet number the characteristic length is set equal to the length of each fracture segment, $L/2$, or, equivalently, half the distance between successive intersections, and the velocity is set equal to the mean velocity inside the fractures, v_f . Fig. 4 shows snapshots of a solute particle ensemble for a moderate and a high Pe value, taken after the same amount of time from the pulse injection moment has elapsed in the two cases. The significance of the mixing and streamline-routing mechanisms, respectively, is apparent. The reference time used in this figure to render time dimensionless is the time needed for the solvent to cross the working domain moving at the mean fracture velocity, that is, L/v_f .

2.4. Lattice Boltzmann advection–diffusion method

Although direct and straightforward in its implementation, the aforementioned lattice Boltzmann–particle-tracking (LB–PT) method may pose severe computational time requirements on the evaluation of the mixing ratio for large Pe values. This is due to the large number of test particles needed to allow for a statistically significant fraction of particles that will deviate from streamline routing. An alternative approach to evaluate the mixing ratio involves the use of a lattice Boltzmann scheme, which contains two evolution equations, one for the carrier fluid and one for the solute. The former is essentially the one typically used in the standard fluid flow LB model, whereas the latter introduces a diffusive mobility of the solute, which shares the convective velocity of the main stream. Such a model was introduced by Dawson et al. [10], working with the hexagonal lattice to simulate flow, diffusion and chemical reaction, whereas Kumar et al. [22] applied it later to simulate Taylor–Aris dispersion in a slit of expansion–contraction geometry, using the nine-speed lattice. A similar approach is presented here and applied to the problem of solute dispersion in the orthogonal intersection of Fig. 1 for the calculation of the M_r value, as discussed below. Stockman et al. [36] used an LB scheme that considers miscible fluids, originally suggested by Flekkøy [12], in order to calculate mixing ratio values in a fracture junction.

According to the LB advection–diffusion model (LB–AD) used in the present work, an arbitrary number M of dissolved species can be introduced into the system having densities $\rho_s, s = 1, \dots, M$. The evolution of the dissolved species is monitored by the following LB equations:

$$f_{s,i}(\mathbf{x} + \mathbf{e}_{s,i}, t + 1) = f_{s,i}(\mathbf{x}, t) + \Omega_{s,i}; \quad i = 0, \dots, 8; s = 1, \dots, M \tag{23}$$

$$\Omega_{s,i} = -\frac{f_{s,i} - f_{s,i}^{eq}}{\tau_s}; \quad i = 0, \dots, 8; s = 1, \dots, M. \tag{24}$$

The densities and velocities of the system are given by the following moments

$$\rho_s(\mathbf{x}, t) = \sum_i f_{s,i}(\mathbf{x}, t) = \sum_i f_{s,i}^{eq}(\mathbf{x}, t) \tag{25}$$

$$\rho_s \mathbf{v}_s(\mathbf{x}, t) = \sum_i f_{s,i}(\mathbf{x}, t) \mathbf{e}_i = \sum_i f_{s,i}^{eq}(\mathbf{x}, t) \mathbf{e}_i. \tag{26}$$

The following constraint is imposed on the velocity of the species

$$\sum_i f_{s,i}^{eq}(\mathbf{x}, t) \mathbf{e}_i = \rho_s \mathbf{v}(\mathbf{x}, t), \tag{27}$$

where \mathbf{v} is the velocity of the solvent. Eq. (27) expresses the fact that the mean velocities of all the species are equal to the mean velocity of the solvent (assumption of dilute solution).

In order to comply with the above constraints, Dawson et al. [10] expressed the equilibrium distribution function of the tracer ($f_{s,i}^{eq}$) in terms of the density ratio of the tracer and the solvent (ρ_s/ρ_0) as

$$f_{s,i}^{eq} = (\rho_s/\rho_0) f_{0,i}^{eq}.$$

Using the Chapman–Enskog procedure, the following equation is recovered for the advection–diffusion D_2Q_9 model [10]

$$\frac{\partial \rho_s}{\partial t} + \nabla \cdot (\rho_s \mathbf{v}) - D_s \nabla^2 \rho_s = 0 \quad s = 1, \dots, M. \tag{28}$$

The mass and momentum balance equations (10) and (11) are written here for the solvent, assuming low concentration of the dissolved species:

$$\frac{\partial \rho_0}{\partial t} + \nabla \cdot (\rho_0 \mathbf{v}) = 0 \tag{29}$$

$$\frac{\partial (\rho_0 \mathbf{v})}{\partial t} + \nabla \cdot (\rho_0 \mathbf{v} \mathbf{v}) = -\nabla P_0 + \rho_0 \mu \nabla^2 \mathbf{v} + O(v^3), \tag{30}$$

where μ is the dynamic viscosity of the solvent.

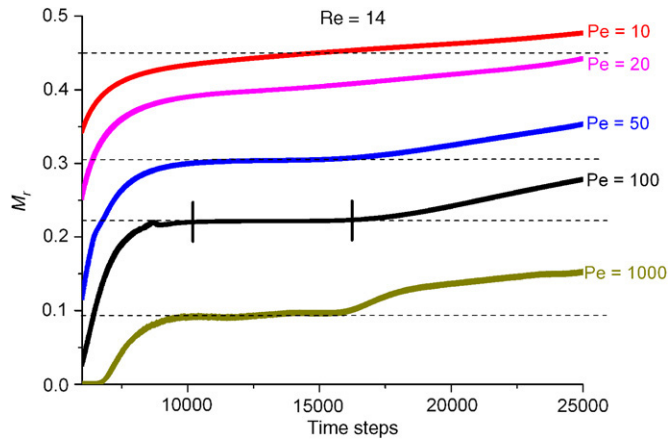


Fig. 5. Dependence of mixing ratio estimates on time in the lattice Boltzmann advection–diffusion model. Effect of the Peclet number. The length is $L = 405$, the fracture width-to-length ratio is 0.05, the kinematic viscosity of the solvent is $\nu = 0.2$ and the diffusivity ranges from $D_m = 2.7 \times 10^{-3}$ to $D_m = 2.7 \times 10^{-1}$.

The diffusion coefficient for the species D_s is given by

$$D_s = c_s^2(\tau_s - 0.5); \quad s = 1, \dots, M, \tag{31}$$

where $c_s^2 = 1/3$.

The Peclet number in our LB scheme is calculated by the expression

$$Pe = v_f L / 2D_s,$$

where v_f is the mean velocity inside the fracture.

In this work, a modified algorithm is used, that sidesteps the simultaneous monitoring of the evolution of the two populations. More specifically, the flow field is calculated first, using the single phase flow LB model. Once fully developed flow is attained, the species evolution equation alone is considered, that simply uses the local velocity field calculated in the first stage. This method was tested first on the Taylor–Aris dispersion problem in a single tube and reproduced accurately the dependence of the longitudinal dispersion coefficient on the mean velocity.

Application of this model to the present problem proceeds as follows. A pulse of the tracer is introduced in the inlet branch (dotted line in Fig. 1) and the population distribution into the outlet branches is monitored as a function of time, using the solute equation alone. The M_r value is extracted from the plateau that is reached (“flux” method) upon convergence (see Fig. 5). Alternatively, one can introduce sink regions at the ends of the outlet branches and evaluate the total amount of solute (“integral” technique) that exits through each one of them. The two types of calculation yield almost identical results for high Pe values. The advantage of the “integral” approach is that it can be used for any Pe value, including moderate and low Pe values, where upstream diffusion becomes significant. In this case, the plateau of Fig. 5 may never be reached and extraction of the M_r value may prove impossible (for $Pe < 5$, according to Fig. 5). This is attributed to the fact that the diffusion process is sufficiently significant to prohibit simultaneous confinement of the solute particles within a single outlet branch at any time instant, which can certainly be the case for elevated Pe values. On the contrary, the “integral” approach will always yield the transfer probability from the inlet branch to any of the four fractures that meet in the intersection. In this case, the incoming population densities are set equal to zero at the fracture exits in order to simulate sink conditions there.

2.5. Solid–fluid boundary conditions for the lattice Boltzmann advection–diffusion model

In the lattice Boltzmann advection–diffusion simulations, the bounce-back scheme was used in both solvent flow and tracer transport processes, as customarily done when using the model by Dawson et al. [10] for advection–diffusion problems (see, for instance, Kumar et al. [22]). The validity of this scheme was also tested by the authors through dispersion simulations in straight tubes and confirmed with excellent accuracy. In fact, the bounce-back rule imposes a no-slip boundary condition for the tracer transport, which is natural for low Knudsen numbers.

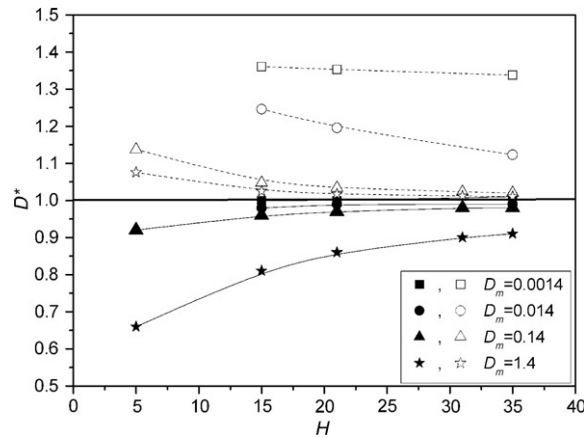


Fig. 6. Normalized diffusion coefficient D^* plotted against the slit gap width (H). The solid lines correspond to the use of the bounce-back rule and the dashed lines to the use of the “bounce-forward” rule. The length is $L = 5000$, the kinematic viscosity of the solvent is $\nu = 0.2$ and the diffusivity ranges from $D_m = 1.4 \times 10^{-3}$ to $D_m = 1.4$.

It has been argued by Drazer and Koplik [11] that the bounce-back rule is inadequate for the simulation of dispersion as it fails to reproduce the correct theoretical diffusion coefficients if the LB-AD model by Flekkøy [12] is used. To remedy this, they suggested a “bounce-forward” boundary condition at the fluid–solid interface, which is implemented through the simple inversion of the normal to the wall component of the fluid velocity, leaving the component that is parallel to the wall unaffected (specular reflection). An investigation of the incorporation of the bounce-forward condition to the LB-AD model used in this work is presented next.

Pure diffusion in a slit of length = 5000 is simulated using both types of boundary condition and various values of the gap width H . The normalized diffusion coefficient D^* is calculated, defined as the ratio of the diffusion coefficient calculated by the simulation (D) to the diffusion coefficient as given in the LB method (D_m),

$$D_m = c_s^2(\tau_D - 0.5), \quad (32)$$

where τ_D is the relaxation parameter of tracer and $c_s^2 = 1/3$.

In Fig. 6 the normalized diffusion coefficient D^* is plotted against the slit gap width (H). According to this figure, the bounce-back rule remains accurate for $H > 15$ provided that $D_m < 1$ whereas the specular reflecting choice fails to predict the correct dimensionless diffusion coefficient. On the contrary, for $D_m > 1$ it seems that the specular reflection rule produces more accurate results. This is attributed to the fact that the $D_m > 1$ region lies beyond the continuum limit of molecular diffusion and extends into the intermediate Knudsen flow regime. The relaxation parameter τ_D is related to the Knudsen number (Kn) of the tracer flow, since the ratio τ_D/H is proportional to Kn . For $D_m = 1$, Kn is of the order of 10^{-1} and, therefore, the mean free path is not negligible compared to the gap width. It is well-known that for moderate and high Knudsen numbers (free molecule flow regime), the assumption of a “slip layer” next to the wall produces realistic results [2]. Therefore, the “bounce-forward” rule, which results in a slip boundary condition, is expected to perform better than the bounce-back condition at elevated Knudsen numbers. However, in our present work, the continuum diffusion regime applies, hence $Kn \rightarrow 0$ and the bounce-back condition remains accurate for the particular LB-AD model used here.

2.6. Stability aspects

Sterling and Chen [35] presented a linear von Neumann stability analysis assuming small spatial fluctuations around a mean “global” equilibrium distribution function. An extensive linear stability analysis has also been presented by Worthing et al. [38]. The authors in both publications have determined stable regions for two LBE-BGK models, namely the seven-speed D_2Q_7 and the nine-speed D_2Q_9 (in the two-dimensional space), examining the wave number of the corresponding Fourier transformed perturbed LB equation, k_x, k_y , the relaxation parameter, τ , the ratios of the rest to moving particles, a in D_2Q_7 and a, b , in D_2Q_9 , and the mesh size. Finer mesh size narrows the stability

region, especially when the relaxation parameter, τ , approaches its limiting value of 0.5. In order to retain stability, the mean flow has to be reduced along with the grid Reynolds and Peclet numbers.

On the other hand, recent advances on stability issues have emerged along with the development of the multi-relaxation-time lattice Boltzmann equation (MRT-LBE) models, first introduced by d’Humières [8]. The MRT-LBE scheme uses individual relaxation parameters for each nonconserved moment, rendering thus the method more stable than the LB-BGK ([24] and [9] in 3D). In that sense, the stability of each nonlinear equilibrium function can be examined, since the nonlinear terms can trigger instabilities even in regions where the linear terms are stable ($\tau < 0.5$; [8]). The MRT-LBE proves to have a broader region of stability than the BGK-LBE, for various relaxation parameters and mean stream velocities. It should be stated that the stability analysis considered in the literature assumes periodic boundary conditions, ignoring thereby the influence of other types of boundary conditions, which in turn may alter significantly the stability behavior [38,24]. Our simulation parameters are well within the stability range that was determined for the LB-BGK model.

For the dispersion simulation the stability of the flow calculation is a necessary but not sufficient condition, since the stability of the tracer transport must also be ensured. However, since the lattice Boltzmann equation for the tracer is the same as the one for the solvent, the same stability constraints should apply for the dispersion part as well. The difference lies with the relation of the relaxation time for the transport problem to the transport property (diffusivity in this case). Specifically, the condition $\tau_D \geq 0.5$ for the tracer relaxation time is now obtained from the requirement that the diffusion coefficient be positive, according to

$$D_m = c_s^2(\tau_D - 0.5).$$

An error analysis for the LB-AD model has been presented by Kumar et al. [22]. In their study they concluded that the error depends on the ratio of the diffusion relaxation parameter to the slit gap width (τ_D/H), which is proportional to the Knudsen number. According to Kumar et al. [22] the error is minimal for $\frac{\tau_D}{H} < 0.08$.

Our calculations revealed excellent agreement with the Taylor–Aris analytical result for $10^{-5} < D_m < 1$ (for $H = 21$). For $D_m < 10^{-5}$ the simulation is unstable, and for $D_m > 1$ the error of the calculated value of D compared to the prescribed value is not negligible, in agreement with the conclusions by Kumar et al. [22] and the argument that the Knudsen number becomes finite. It must be mentioned that all LB-AD calculations and graphs presented in this work were obtained using D_m values within the aforementioned range.

2.7. Calculation of the transverse dispersion coefficient

In a regular square network of straight fractures, the overall transverse dispersion coefficient can be calculated from the following expression, which makes use of the mixing ratio values at the level of a single intersection, as discussed above:

$$\frac{D_T}{D_m} = \frac{1}{2} \frac{M_r}{1 - M_r} Pe. \quad (33)$$

Eq. (33) is valid for an angle 45° between the principal network axes and the macroscopic flow direction. This equation was also suggested by Park et al. [32] as a best fit to their calculations.

3. Results and discussion

For the calculation of the mixing ratio with the LB–PT method, the trajectory of each test particle is monitored as it starts from an inlet branch and eventually exits through any of the outlet branches. The total number of particles needed for each simulation depends strongly on the Pe value and on the required accuracy. In order to investigate the convergence dynamics, the M_r value and the corresponding D_T value, obtained from Eq. (33) are monitored at gradually increasing number of test particles. The converging process for $M_w = 0.1$ and two Pe values (10^2 and 10^4) can be observed in Fig. 7 for two random realizations. Faster convergence is achieved at the higher Pe value, as only 10,000 test particles proved sufficient for the calculation of the M_r value. However, increased accuracy in the M_r value is required as Pe increases in order to produce stable and accurate predictions of the D_T value, according to Eq. (33). This is due to the fact that $M_r \rightarrow 0$ as Pe increases, thus rendering the precise evaluation of D_T from Eq. (33) quite demanding computationally.

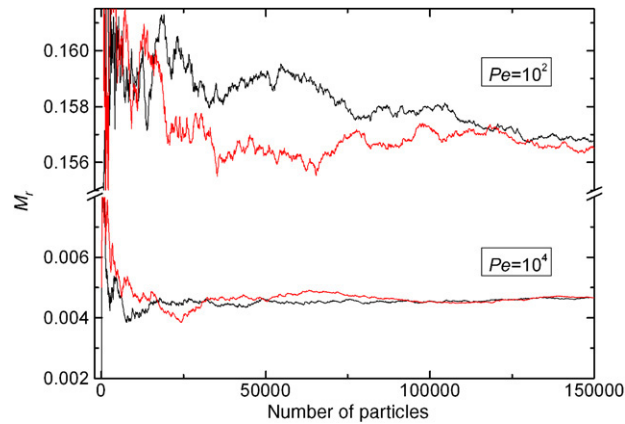


Fig. 7. Convergence behavior of the M_r values at increasing sampling, for $Pe = 10^2$ and $Pe = 10^4$.

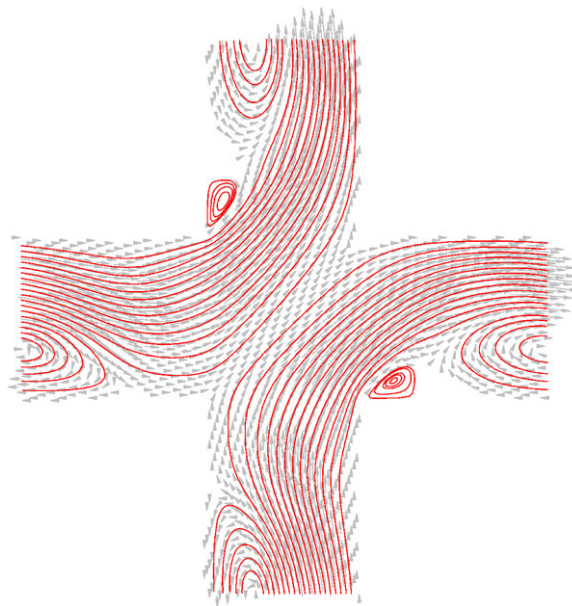


Fig. 8. Streamlines in an intersection at elevated Reynolds number ($Re = 116$), indicating extended recirculation regions. Fracture width-to-length ratio: 0.3, the length is $L = 205$ and the kinematic viscosity is $\nu = 0.06$.

In addition to the widely known strong dependence of the dispersion coefficient on the Peclet number value, there is a strong dependence on the Reynolds number as well. The Reynolds number is defined using the mean velocity in a fracture as characteristic velocity and the width of the fracture as the characteristic length. In fact, one can alter the Reynolds number without changing the Peclet number, provided that the molecular diffusion coefficient is adjusted accordingly. Our results indicate that for Reynolds number higher than ~ 70 , the dispersion coefficient decreases drastically with increasing Reynolds number, despite the fact that the Peclet number is kept constant. This is attributed to the generation of stationary vortices in regions close to the intersection, obviously due to the sharp wall corner that exists there (Fig. 8). The dependence of the transverse dispersion coefficient, as obtained with the use of Eq. (33), on the Peclet number is shown in Fig. 9. In the same figure, the effect of the Reynolds number on the dispersion coefficient is also presented. The aforementioned vortices tend to temporarily “trap” solute particles, thus limiting their displacement in directions lateral to the macroscopic flow direction, provided of course that some diffusive motion is allowed so that they can switch from the main stream lines to the vortex regions.

The predictions of the LB–PT method for the mixing ratio in an orthogonal intersection compare well with those by Stockman et al. [36], over the entire Peclet number range, as shown in Fig. 10. A comparison between the predictions

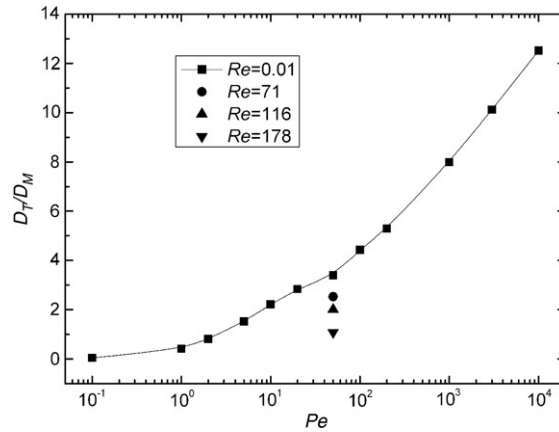


Fig. 9. Dependence of the transverse dispersion coefficient on the Reynolds number for various values of the Peclet number.

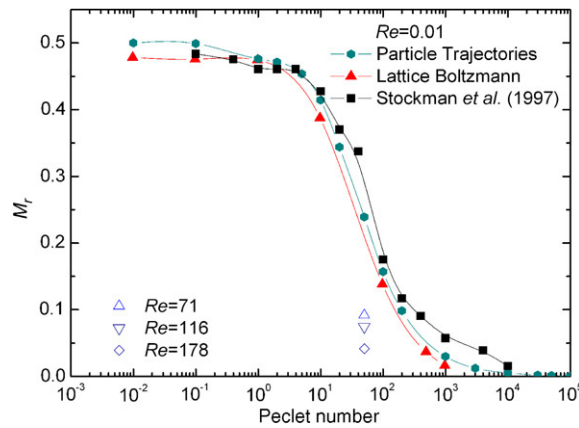


Fig. 10. Comparison of the mixing ratio obtained by the lattice Boltzmann–particle-tracking method (dot symbols) to that obtained by the lattice Boltzmann advection–diffusion model (triangle symbols) and to literature results (square symbols). Fracture width-to-length ratio: 0.1; $Re < 0.1$; $L = 205$; $\nu = 0.2$.

of the LB–PT method and those of the LB–AD method for the mixing ratio in an intersection of relatively narrow fractures (width-to-length ratio: 0.1) is also shown in this figure over a wide range of Pe values. In this particular set of calculations, flow is sufficiently slow to exclude the generation of vortices and ensure almost creeping flow conditions (Reynolds number $\approx 10^{-7}$). Notice the very satisfactory agreement between the two sets of results, except for the very high Pe region. This small deviation may be attributed to the fact that the calculations are in this region extremely sensitive to the precise value of the diffusion coefficient, and lattice size effects as well as statistical errors in the stochastic simulation may become very significant.

As already mentioned above, there is a concrete advantage in the use of the LB–AD method for the evaluation of the mixing ratio at an intersection, compared to that of the LB–PT approach. Namely, the latter, although conceptually rigorous, may require large computational times for high Pe values because of the stochastic nature of the computational procedure. Specifically, as the Peclet number increases, the number fraction of solute particles that keep moving straight ahead into the opposite outlet branch decreases; consequently, a progressively larger number of test particles is needed to eliminate statistical errors. On the other hand, the LB–AD method is insensitive to this phenomenon, since it considers continuum quantities only and calculates directly the evolution of the tracer in a deterministic fashion.

Fig. 11 shows the evolution of some representative contours of constant solute concentration, as predicted by the LB–AD approach. At the specific Pe value indicated there ($Pe = 100$), convection is sufficiently strong to ensure the existence of a time window, during which the entire solute tracer lies within the two outlet branches. Thus, the

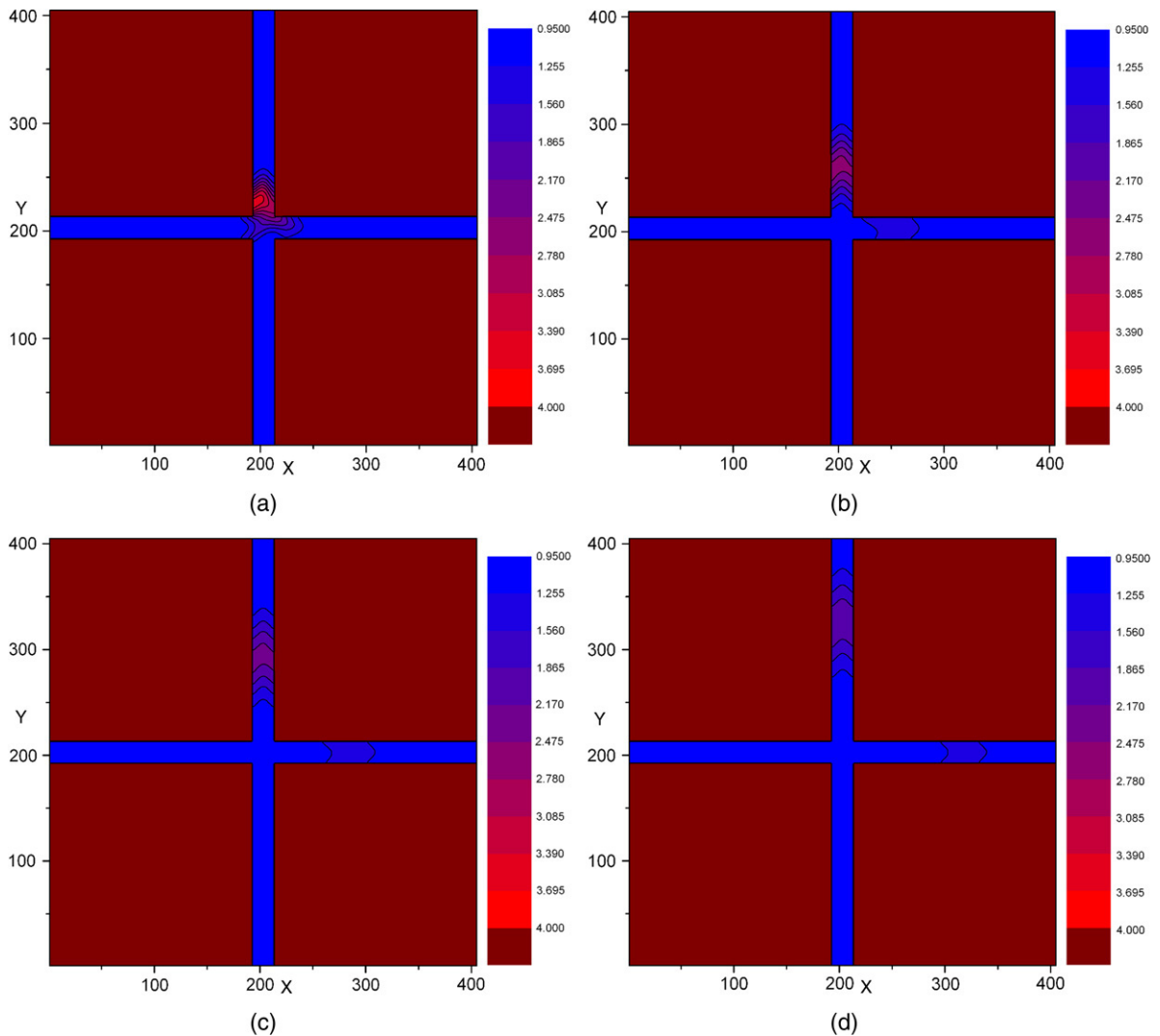


Fig. 11. Contours of solute concentration in an intersection. $Pe = 100$; $Re = 1.4$, fracture width-to-length ratio: 0.05. The rest of the simulation data are the same as in Fig. 5.

magnitude of the plateau of Fig. 5 is sufficient to allow the evaluation of the mixing ratio. However, for lower Pe values, this may not be the case, as already mentioned above. To remedy this, the “integral” approach can be used, as explained above. In this case, the computation of the mixing ratio always converges, provided that sufficient time is allowed. The length is $L = 205$, the fracture width-to-length ratio is 0.05, the kinematic viscosity of the solvent is $\nu = 0.2$ and the diffusivity ranges from $D_m = 2.7 \times 10^{-3}$ to $D_m = 5.4 \times 10^{-1}$. About 30,000 time steps are needed for the convergence of the calculated mixing ratio value to its final value for all moderate and high Pe values considered here (Fig. 12). This lack of sensitivity to the Pe value renders this method more practical than the particle-tracking method in the high Pe region ($Pe > 100$). Note also that the final value of the mixing ratio is insensitive to the precise positioning of the pulse within the inlet branch.

4. Conclusions

A lattice Boltzmann approach was used here to compute the flow field in an orthogonal intersection of fractures that are inclined by 45° with respect to the macroscopic flow direction. Subsequently, a particle-tracking method was used to yield mixing ratio values at the intersection scale, which can then be used for the evaluation of the network-scale transverse dispersion coefficient. For high Peclet number values, this methodology may prove computationally

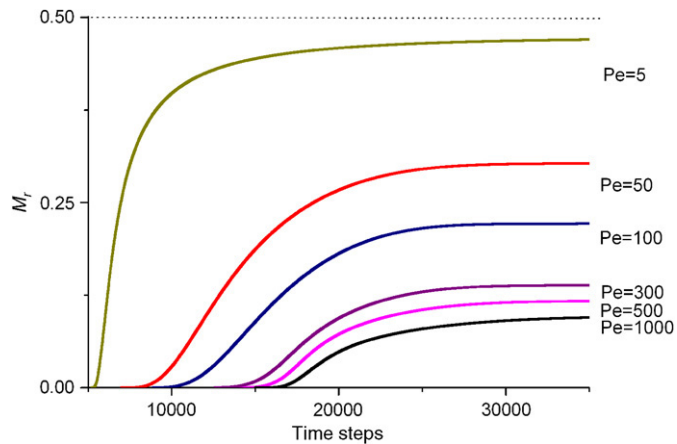


Fig. 12. Estimates of the mixing ratio in an intersection using the lattice Boltzmann advection–diffusion model vs. number of time steps. Variation with the Peclet number. $Re = 1.4$; fracture width-to-length ratio: 0.05.

expensive if accurate mixing ratio values are pursued. To circumvent this problem, a lattice Boltzmann method was used that monitors the evolution of a solute pulse inside the intersection and the emanating fractures, which has the advantage over the particle-tracking method to converge to the final mixing ratio value at a speed that is practically insensitive to the Pe value, even in the high Pe region, without sacrificing accuracy.

More specifically, the M_r values calculated using the LB-AD method have been obtained with two different approaches, namely the “flux” scheme, where the M_r value is extracted from the plateau that is reached in the M_r vs. simulation time graph, and the “integral” scheme, where the total amount of solute that exits through each one of the branches is evaluated. The former scheme is faster than the “integral” scheme but suffers from the drawback that such a plateau may not appear at low Pe values ($Pe < 5$). On the other hand, the “integral” scheme is faster by one order of magnitude than the LB-PT method for low Pe values, but becomes considerably slower (also by one order of magnitude or more) than it at high Pe values. However, in the high Pe region, the “flux” LB-AD method is to be preferred over the “integral” one, as it proves faster by $\sim 33\%$ than the LB-PT method.

The tracer-wall interaction was simulated here using the bounce-back algorithm, which was validated first in the limit of the classical Taylor–Aris dispersion in a straight tube. Use of the “bounce-forward” (specular reflection) scheme produced tracer slip on the wall, which is justified for elevated Knudsen numbers only. The calculations appeared stable over a wide range of the diffusion relaxation time, which corresponds to the diffusivity range $10^{-5} < D_m < 1$.

An important conclusion regarding sensitivity of the mixing process to the Reynolds number was also drawn. Specifically, it was shown that for applications that involve fast flows, the precise value of the Reynolds number is of critical importance in the evaluation of the mixing ratio in an intersection and, consequently, of the dispersion coefficient. In other words, the convenience of changing the Pe value through a change in the diffusion coefficient alone in order to avoid recalculation of the flow field may lead to erroneous results in fast flow cases. The generation of stationary vortices at Reynolds number higher than 70 appears to affect drastically the transport of the solute particles, which may be trapped into the recirculation regions and confine themselves there for substantial amounts of time, thus lowering significantly the dispersion coefficient.

Acknowledgment

Financial support has been provided by the “Competitiveness” Programme, project 04AKMON61, co-funded by EU and the Hellenic General Secretariat for Research and Technology.

References

- [1] B. Berkowitz, C. Naumann, L. Smith, Mass transfer at fracture intersections: An evaluation of mixing models, *Water Resour. Res.* 30 (1994) 1765–1773.

- [2] A. Beskok, G.E. Karniadakis, A model for flows in channels, pipes and ducts at micro and nano scales, *Microscale Thermophys. Eng* 3 (1999) 43–77.
- [3] B. Bijeljic, A.H. Muggeridge, M.J. Blunt, Pore-scale modeling of longitudinal dispersion, *Water Resour. Res.* 40 (2004) W11501.
- [4] P.L. Bhatnagar, E.P. Gross, M. Krook, A model for collision processes in Gases. I. Small amplitude processes in charged and neutral one-component systems, *Phys. Rev. E* 94 (1954) 511–525.
- [5] J.M. Buick, C.A. Greated, Gravity in the lattice Boltzmann model, *Phys. Rev. E* 61 (2000) 5307–5320.
- [6] V.N. Burganos, Gas diffusion in random binary media, *J. Chem. Phys.* 109 (1998) 6772–6779.
- [7] S. Chapman, T.G. Cowling, *Mathematical Theory of Non-Uniform Gases*, Cambridge University Press, Cambridge, 1939.
- [8] D. D’Humières, Generalized lattice-Boltzmann equations, in: *AIAA Rarefied Gas Dynamics: Theory and Simulations*, in: *Progress in Astronautics and Aeronautics*, vol. 59, 1992, pp. 450–548.
- [9] D. D’Humières, I. Ginzburg, M. Kraczyk, P. Lallemand, L.S. Luo, Multiple-relaxation-time lattice Boltzmann models in three dimensions, *Philos. Trans. R. Soc. A* 360 (2002) 437–451.
- [10] S.P. Dawson, S. Chen, G.D. Doolen, Lattice Boltzmann computations for reaction–diffusion equations, *J. Chem. Phys.* 98 (1993) 1514–1523.
- [11] G. Drazer, J. Koplik, Tracer dispersion in two-dimensional rough fractures, *Phys. Rev. E* 63 (2001) 056104.
- [12] E.G. Flekkøy, Lattice Bhatnagar–Gross–Krook models for miscible fluids, *Phys. Rev. E* 47 (1993) 4247–4257.
- [13] U. Frisch, B. Hasslacher, Y. Pomeau, Lattice-Gas automata for the Navier–Stokes equation, *Phys. Rev. Lett.* 56 (1986) 1505–1508.
- [14] Z. Guo, C. Zheng, B. Shi, Discrete lattice effects on the forcing term in the lattice Boltzmann method, *Phys. Rev. E* 65 (2003) 046308.
- [15] F.J. Higuera, J. Jimenez, Boltzmann approach to lattice gas simulations, *Europhys. Lett.* 9 (1989) 663–668.
- [16] P. Gaganis, E.D. Skouras, M.A. Theodoropoulou, C.D. Tsakiroglou, V.N. Burganos, On the evaluation of dispersion coefficients from visualization experiments in artificial porous media, *J. Hydrol.* 307 (2005) 79–91.
- [17] I. Ginzbourg, P.M. Adler, Boundary flow condition analysis for the three dimensional lattice Boltzmann model, *J. Physique II* 4 (1994) 191–214.
- [18] X.Y. He, Q. Zou, L.-S. Luo, M. Dembo, Analytic solutions of simple flows and analysis of non-slip boundary conditions for the lattice Boltzmann BGK model, *J. Stat. Phys.* 87 (1997) 115–136.
- [19] J.O. Hirschfelder, C.F. Curtis, R.B. Bird, *Molecular Theory of Gases and Liquids*, Wiley, New York, 1964.
- [20] S. Hou, Q. Zou, S. Chen, G. Doolen, A.C. Cogley, Simulation of cavity flow by the Lattice Boltzmann method, *J. Comput. Phys.* 118 (1995) 329–347.
- [21] A.N. Kalarakis, V.N. Burganos, A.C. Payatakes, Galilean-invariant lattice-Boltzmann simulation of liquid–vapor interface dynamics, *Phys. Rev. E* 65 (2002) 0567021–05670213.
- [22] R. Kumar, S.S. Nivarthi, H.T. Davis, D.M. Kroll, R.S. Maier, Application of the lattice Boltzmann method to study flow and dispersion in channels with and without expansion and contraction geometry, *Int. J. Numer. Meth. Fluids* 31 (1999) 801–819.
- [23] A.D. Ladd, R. Verberg, Lattice-Boltzmann simulations of particle-fluid suspensions, *J. Stat. Phys.* 104 (2001) 1191–1251.
- [24] P. Lallemand, L.S. Luo, Theory of the lattice Boltzmann method: Dispersion, dissipation, isotropy, Galilean invariance, and stability, *Phys. Rev. E* 61 (2000) 6546–6562.
- [25] G. Li, Tracer mixing at fracture intersections, *Environ. Geol.* 42 (2002) 137–144.
- [26] L.-S. Luo, Analytic solutions of linearized lattice Boltzmann equation for simple flows, *J. Stat. Phys.* 88 (1997) 913–926.
- [27] L.-S. Luo, Unified theory of lattice Boltzmann models for nonideal gases, *Phys. Rev. Lett.* 81 (1998) 1618–1621.
- [28] R.S. Maier, D.M. Kroll, R.S. Bernard, S.E. Howington, J.F. Peters, T.D. Davis, Pore-scale simulation of dispersion, *Phys. Fluids* 12 (2000) 2065–2079.
- [29] V.V. Mourzenko, F. Yousefian, B. Kolbah, J.F. Thovert, P.M. Adler, Solute transport at fracture intersections, *Water Resour. Res.* 38 (2002) 1000.
- [30] D.R. Noble, S. Chen, J.G. Georgiadis, R.O. Buckius, A consistent hydrodynamic boundary condition for the lattice Boltzmann method, *Phys. Fluids* 7 (1995) 203–209.
- [31] Y.J. Park, K.K. Lee, Analytical solutions for solute transfer characteristics at continuous fracture junctions, *Water Resour. Res.* 35 (1999) 1531–1537.
- [32] Y.J. Park, K.K. Lee, B. Berkowitz, Effects of junction transfer characteristics on transport in fracture networks, *Water Resour. Res.* 37 (2001) 909–923.
- [33] Y.H. Qian, D. D’Humières, P. Lallemand, Lattice BGK models for Navier–Stokes equation, *Europhys. Lett.* 17 (1992) 479–484.
- [34] J. Salles, J.F. Thovert, R. Delannay, L. Prevors, J.L. Auriault, P.M. Adler, Taylor dispersion in porous media. Determination of the dispersion tensor, *Phys. Fluids A* 5 (1993) 2348–2376.
- [35] J.D. Sterling, S.Y. Chen, Stability analysis of lattice Boltzmann methods, *J. Comput. Phys.* 123 (1996) 196–206.
- [36] H.W. Stockman, C. Li, J.L. Wilson, A lattice-gas and lattice Boltzmann study of mixing at continuous fracture junctions: Importance of boundary conditions, *Geophys. Res. Lett.* 24 (1997) 1515–1518.
- [37] S. Succi, E. Foti, F. Higuera, Three-dimensional flows in complex geometries with the lattice Boltzmann method, *Europhys. Lett.* 10 (1989) 433–438.
- [38] R.A. Worthing, J. Mozer, G. Seeley, Stability of lattice Boltzmann methods in hydrodynamic regimes, *Phys. Rev. E* 56 (1997) 2243–2253.
- [39] Q.S. Zou, X. He, On pressure and velocity boundary condition for the lattice Boltzmann BGK model, *Phys. Fluids* 9 (1997) 1591–1598.